Dalton Transactions

ROYAL SOCIETY OF CHEMISTRY

PAPER

View Article Online
View Journal

Cite this: DOI: 10.1039/d1dt01585k

Alternative ball-milling synthesis of vanadium-substituted polyoxometalates as catalysts for the aerobic cleavage of C–C and C–O bonds†

Louay Al-Hussaini,[a,b] Sabine Valange,[c] Maria Elena Gálvez *[b] and Franck Launay *[a]

Vanadium-substituted phosphomolybdic acids ($H_{3+x}[PMo_{12-x}V_xO_{40}]$, denoted as V_x) are well-known oxidation catalysts that are generally prepared by the hydrothermal treatment of MoO_3 and V_2O_5 in the presence of H_3PO_4. This synthesis procedure is highly energy consuming and the V_x yields are not always acceptable. In the present work, an alternative hybrid mechanochemical/hydrothermal synthesis of V_x is proposed, comprising the ball-milling of MoO_3 and V_2O_5, followed by a hydrothermal attack. The resulting materials, with $2 \leq x \leq 3$, obtained from this new route were compared, in terms of yield, energy consumption and catalytic activity, with a reference V_3 sample prepared through a conventional hydrothermal treatment. The ball-milling step proved to lead not only to a shorter and far more energy-saving synthesis procedure, but also to high yields of V_x. Moreover, V_x from this alternative route proved to be generally more active than the conventionally prepared V_3 in the aerobic oxidative cleavage of C–O and C–C bonds in 2-phenoxyacetophenone, used herein as a lignin model compound.

Received 16th May 2021,
Accepted 30th July 2021

DOI: 10.1039/d1dt01585k

rsc.li/dalton

Introduction

Vanadium-substituted phosphomolybdic acids, $H_{3+x}[PMo_{12-x}V_xO_{40}]$ – denoted as V_x – have been widely used as catalysts in different aerobic oxidation reactions.[1] Among them, the cleavage of C–C and C–O bonds[2] has several interesting applications, such as in the aerobic delignification of wood pulp[3] or lignin depolymerisation[4] leading to the production of aromatics from biomass.[5] Usually, V_x catalysts are synthesized either from their corresponding metal salts through the "etherate" route,[6] or from their metal oxides, following a hydrothermal[7,8] or an "oxo-peroxo"[9] route (Fig. 1). Though widely used, the "etherate" pathway involves strong acids, as well as diethyl ether, a flammable, harmful and environmentally hazardous solvent. The "oxo-peroxo" route, involving the attack of the starting oxides by hydrogen peroxide, is less developed, since it generally leads to the formation of rather unstable vanadium complexes. On the other hand, the hydrothermal route has been often preferred, because it is a relatively simple procedure that consists of the acidic attack of the starting oxides in refluxing water.[7,8] However, this route still requires long reaction times and works under very diluted conditions, especially when high vanadium contents are targeted. The rate-limiting step seems to be the acidic attack of the starting MoO_3 and V_2O_5 oxides.

Ball-milling has attracted growing interest in recent years[10] for applications such as solvent-free reactions,[11–15] and the activation of oxides,[16,17] carbonates[18] and dioxygen,[19] as well

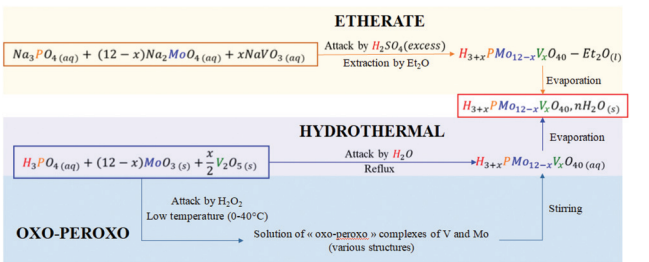

Fig. 1 Main conventional procedures for the synthesis of vanadium-substituted phosphomolybdic acids (V_x).

[a]Sorbonne Université, CNRS, UMR 7197, Laboratoire de Réactivité de Surface (LRS), F-75005 Paris, France. E-mail: franck.launay@sorbonne-universite.fr
[b]Sorbonne Université, CNRS, UMR 7190, Institut Jean le Rond d'Alembert, F-75005 Paris, France. E-mail: elena.galvez_parruca@sorbonne-universite.fr
[c]Institut de Chimie des Milieux et Matériaux de Poitiers (IC2MP), Université de Poitiers, CNRS, ENSI Poitiers, B1, 1 rue Marcel Doré, F-86073 Poitiers Cedex 9, France

†Electronic supplementary information (ESI) available: Weights engaged and elemental analyses of the different V_x prepared; Comparison of the XRD profiles of V_3-HT with a JCPDS reference and Rietveld refinement results; the TGA profiles of all V_x catalysts; the proportion of the different isomers in V_2 measured by ^{31}P NMR, XRD and ^{31}P NMR analysis of V_2-BM_{20} materials; details on energy consumption; the XRD profiles of all the precursors of V_2-BM_{50} and V_2-BM_{20}; the estimation of the crystallite size; the synthetic procedure of **K**; an example of HPLC profile; calibration curves. See DOI: 10.1039/d1dt01585k

as for the synthesis of a variety of composites,[20] organometallics,[21] MOFs[22] and metallic compounds,[17,23] *i.e.* amorphous and nano-structured materials[22,24,25] for catalytic[22] and energy-related applications.[24–26] In the field of catalysis, Zazhigalov *et al.* reported that a mixed oxide of vanadium and molybdenum (MoV_2O_8) synthesized by milling MoO_3 and V_2O_5 single oxides was a much more active catalyst for benzene oxidation into maleic anhydride than the parent oxides.[27] To the best of our knowledge, there is only one example of V_x synthesis using a ball-milling step reported in the literature.[28] Molchanov *et al.* showed that V_x may be prepared through the hydrothermal attack of a ball milled mixture of V_2O_5 and MoO_3 with H_3PO_4 at 80 °C.[28] The authors studied the influence of the duration of the milling step for $x = 4$, the proportions of the starting oxides and the H_3PO_4 attack conditions. It has also to be noted that the authors also tried to carry out the whole synthesis of V_3 in a miller using a two-step procedure (first MoO_3 and V_2O_5, followed by the addition of H_3PO_4). The synthesized V_x compounds were characterized in the solid state by FT-IR, ^{31}P and ^{51}V MAS NMR, but no information was reported on their speciation in solution. Moreover, the V_x materials synthesized through this route were never tested as catalysts, not even characterized in view of their application in catalysis. Other recent studies on polyoxometalates and mechanochemistry have also been reported in the literature[29,30] by Xu *et al.*[29] and Leng *et al.*,[30] but the synthesis of polyoxometalates was carried out using conventional procedures and not by ball-milling.

The literature survey reveals that the hybrid synthesis procedure (ball-milling and subsequent hydrothermal treatment) has scarcely been explored for the preparation of V-polyoxometalates. Such a hybrid pathway can however represent a more sustainable approach for V_x synthesis than the 100% hydrothermal route, requiring less energy and no additional reactant/solvent. In view of this, the present work aims at studying various hybrid synthesis procedures of V_x involving a mechanochemical step (BM–HT) and comparing them with the 100% hydrothermal route (HT), with a focus on the molecular structure and yield of the vanadium-substituted polyoxometalates produced. We further assessed their catalytic activity and selectivity in the aerobic cleavage of a 2-phenoxyacetophenone (**K**), used as a lignin model compound. Special emphasis was also put on the determination of the energy consumption of both processes. V_x with $x = 2$ or 3 were targeted, since with a higher vanadium content the $PMoV_x$ compounds are known to be more unstable especially at high temperatures.[1] In the next step, the physicochemical features of the oxide mixtures obtained upon ball-milling of the starting V_2O_5 and MoO_3 oxides were also investigated, with the aim of evaluating the relevance of the mechanochemical step in the synthesis process. Gaining further knowledge on this hybrid mechanochemical method can provide valuable information about the feasibility of this route for the synthesis of V_x materials.

Experimental

Material synthesis

A reference V_3 material, denoted as V_3-HT, was synthesized[4] through the attack of MoO_3 (Acros Organics) and V_2O_5 (Sigma-Aldrich) by H_3PO_4 (purity 85%, Carlo Erba) in refluxed water, following a procedure adapted from that described by Kern *et al.*[7] In this synthesis, 0.39 g (3.3 mmol) of 85% H_3PO_4 was dissolved in 200 mL of deionized water, followed by the addition of 3.93 g of MoO_3 (27.3 mmol) and 0.92 g (5.1 mmol) of V_2O_5 (Tables 1 and S1†). Compared to the procedure reported earlier by Kern and co-workers and dedicated to the synthesis of V_1-HT only,[7] a longer hydrothermal attack (6.5 h instead of 3 h) and more diluted conditions have been used in our work due to the higher value of x. After cooling, the residual oxides were removed by filtration and water was then evaporated from the filtrate, yielding an orange powder.

In the hybrid BM–HT route, the ball milling step was carried out in a Fritsch Pulverisette 7 planetary miller (jar diameter: 140 mm) using zirconium oxide balls (∅ = 10 mm, weight: 68 g) placed inside a zirconium oxide coated autoclave. The rotation speed was set to 700 rpm and the ZrO_2 ball/oxide weight ratio, denoted as r, was either 20 or 50. For $r = 50$, the

Table 1 Summary of the synthesized V_x materials, conditions with the values of x_{exp} and the yields[a]

Synthesis procedure	V_x	r[b]	t_{BM}[c] (h)	t_{HT}[d] (h)	T (°C)	x_{exp}[e]	Yield[f] (%)
HT	V_3-HT[d]	—	0	6.5	100	2.7	79
BM_{50}	V_3-BM_{50}-1_{BM}-1.5_{HT}	50	1	1.5	80	2.8	97
	V_2-BM_{50}-1_{BM}-1.5_{HT}					1.9	95
BM_{20}	V_2-BM_{20}'-1_{BM}-1.5_{HT}	20	1	1.5	100	2.1	96
	V_2-BM_{20}-1_{BM}-3_{HT}		1	3	80	2.3	97
	V_2-BM_{20}-2_{BM}-1.5_{HT}		2	1.5	80	2.0	96
	V_2-BM_{20}-2_{BM}-3_{HT}		2	3		2.3	95
	V_2-BM_{20}-4_{BM}-1.5_{HT}		4	1.5		2.3	96
	V_2-BM_{20}-4_{BM}-3_{HT}		4	3		2.2	98

[a] The weights of V_2O_5, MoO_3 and H_3PO_4 85 wt% employed for each synthesis are detailed in Table S1† and the elemental analyses of the resulting materials. [b] Ball/oxide weight ratio (r) with zirconium oxide balls (∅ = 10 mm, weight: 68 g). The rotation speed was set to 700 rpm. [c] t_{BM} = ball milling duration. [d] t_{HT} = hydrothermal treatment duration. [e] Determined from ICP, relative error = 10%. [f] Calculated from ^{31}P NMR (±10%).

milling duration (t_{BM}) was fixed to 1 h and the ball milled mixture with nominal theoretical x values (x_{th}) equal to 2 or 3 was subsequently attacked by phosphoric acid in water at 80 °C during t_{HT} = 1.5 h, affording the series of V_x-BM_{50}-1_{BM}-1.5_{HT} materials (see Tables 1 and S1†). Another series of materials (V_2-BM_{20}-t_{BM}-t_{HT}) were prepared for a nominal value of x_{th} equal to 2 and with r = 20 (weight of balls kept constant) but t_{BM} was varied from 1 to 4 h and the ball-milled mixture was attacked during either t_{HT} = 1.5 h or 3 h at 80 °C (unless otherwise specified) (see Tables 1 and S1†).

A preliminary one-pot 100% ball-milling procedure where MoO_3, V_2O_5 and H_3PO_4 were introduced together was attempted (1 h, 700 rpm) for both ball/oxide weight ratios (see Table S1†). The synthesis was successful for r = 50. However, the zirconia balls were severely damaged, thereby resulting in a high contamination of the final product with ZrO_2 as shown by XRD. Such eroded ZrO_2 had to be eliminated by centrifugation in water (7500 rpm, 10 min).

Generally, the mixture of the starting oxides, initially clear brown, turned dark brown after milling. Upon the addition of the solid to the aqueous solution containing a stoichiometric amount of H_3PO_4, the mixture turned red on the first few seconds of the acid attack. At the end, the suspension was filtered to eliminate the residual traces of zirconium oxide originating from the abrasion of the balls, and then water was evaporated to get the V_x solids.

Physicochemical characterization

X-ray powder diffraction analyses (XRD) were performed on a Bruker Advance D8 diffractometer, using a Cu Kα radiation source (λ = 1.5406 Å) without a monochromator. The diffraction patterns were collected from 5° to 50°, at a scanning rate of 0.34° min^{-1}. The crystalline phases were identified by Rietveld analysis of the diffraction patterns (factors R_P and Chi_2), using the Fullprof software. Liquid ^{31}P nuclear magnetic resonance (NMR) analyses were performed on a 400 MHz Bruker apparatus. 30 mg of the solid was dissolved in 250 µL of D_2O (Euriso-top) and 250 µL of H_2O. Then 7.5 µL of dioxane (SDS, Carlo-Erba) was added to the solution. For each analysis, 16 scans were recorded with a relaxation delay of 32 s. The P, Mo and V contents for all samples were determined by inductive coupled plasma analyses (ICP) from Crealins (Lyon, Villeurbanne France) on an ICP Thermo-Fischer iCAM. Thermogravimetric analyses (TGA) were performed on a Cp SDTQ600 system, in order to determine the hydration index of V_x, denoted as n. The temperature was increased up to 600 °C at a heating rate of 10 °C min^{-1} under an air flow of 100 mL min^{-1}. Scanning electron microscopy analyses (SEM) were carried out using a Hitachi SU-70 microscope. The sample was introduced at 3.2 mm from the electron beam source, the accelerating voltage was set to 1 kV and the intensity of the emission current was set to 47 µA. Particle size (granulometry) measurements were performed on a Fristch Analysette 22 Nano Tec. Raman spectroscopy analyses were performed using a RamanRXN spectrometer equipped with a laser working at λ = 785 nm, with a power of 10–12 mW and a resolution of 4 cm^{-1}. The duration of each scan was 10 s and the number of scans was set to 30.

Catalytic experiments and monitoring

In the aerobic cleavage catalytic experiments, 2-phenoxyacetophenone (0.32 g, 1.5 mmol) and V_x (Mo + V, 18 mol%) were dissolved in 15 mL of MeCN/AcOH 90–10 in a Schlenk tube connected to a gas burette system to monitor the dioxygen consumption. The Schlenk tube was purged and then heated during 24 h at 82 °C. After cooling the reaction mixture, an aliquot of 0.5 mL was withdrawn and dropped in a 20 mL volumetric flask and diluted with H_2O–MeOH–AcOH 49 : 49 : 2 for HPLC analysis (Shimadzu LC-20AD) using a Shim-pack XR-ODS column (4.6 × 100 mm, 2.2 µm) heated to 40 °C in a CT0-10AS oven. The mobile phase was composed of aqueous AcOH (0.5 vol%) and methanol (HPLC grade, VWR Chemicals) used at a flow rate of 0.4 mL min^{-1} (0–13 min: 60–40 (MeOH), 13–17 min: gradient from 40 to 60% of methanol, 17–33 min: 40–60 (MeOH), 33–37 min: gradient from 60 to 40% of methanol and 37–50 min: 60–40 (MeOH)). The compounds were detected by using an SPD-M20A UV detector (210 and 220 nm). Benzaldehyde, benzoic acid and phenol were quantified according to the calibration curves (ESI†).

Results and discussion

Influence of the synthesis conditions on the V_x materials

The first series of V_x compounds were synthesized using the hybrid ball milling-hydrothermal procedure (BM–HT) with a ZrO_2 ball/oxide weight ratio r = 50, a milling duration of 1 h and an acid attack duration of the ball-milled mixture of 1.5 h.

Fig. 2a shows the powder XRD patterns of V_2-BM_{50}-1_{BM}-1.5_{HT} and V_3-BM_{50}-1_{BM}-1.5_{HT}, together with the pattern acquired for conventionally synthesized V_3-HT. These patterns were compared to the JCPDS 00-043-0317 reference for

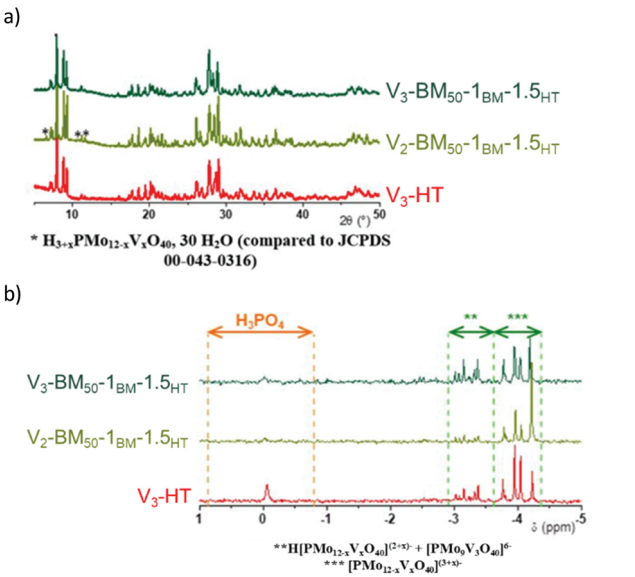

Fig. 2 (a) Powder-XRD patterns and (b) liquid ^{31}P NMR spectra (D_2O/H_2O/dioxane, pH = 1) of V_x-BM_{50}-1_{BM}-1.5_{HT} and V_3-HT materials.

$H_3PMo_{12}O_{40}\cdot 13H_2O$ (Fig. S1 in the ESI†). Both V_x-BM_{50}-1_{BM}-1.5_{HT} materials showed a typical Keggin structure, as evidenced by the presence of diffraction peaks at *ca.* $2\Theta = 8°$, at 15–18° and at *ca.* 28° in all XRD patterns. A closer look at the diffractograms indicated that the crystalline structure was more impacted by the hydration index n than by the vanadium content.[31–33] In V_3-BM_{50}-1_{BM}-1.5_{HT}, one single crystalline phase could be identified, similarly to V_3-HT, but yielding slightly different Rietveld refinement parameters (R_P = 10 and Chi_2 = 2.4 for V_3-BM_{50}-1_{BM}-1.5_{HT}, R_P = 15 and Chi_2 = 13 for V_3-HT, see Table S2 in the ESI†). On the other hand, V_2-BM_{50}-1_{BM}-1.5_{HT} appeared to be constituted of at least two V_x crystalline phases differing in their hydration index, n. The main phase corresponds to n = 13, also present in V_3-HT, whereas the secondary phase corresponds to n = 30 (Fig. 2a, JCPDS 00-043-0316).

The synthesis of vanadium-substituted phosphomolybic acids generally leads to mixtures of different V_x stoichiometries, with x representing the average number of vanadium equivalents. A non-total incorporation of vanadium into the $H_{3+x}[PMo_{12-x}V_xO_{40}]$ structure results in lower values of x, *vis-à-vis* the nominal V-loading (x_{th}), together with the presence of water-insoluble V_2O_5 residues at the end of the synthesis. ICP analyses allowed us to determine the experimental values of x in this series of materials. The theoretical (x_{th}) and experimental (x_{exp}) V_x stoichiometries, as well as the elemental composition in wt% of the polyoxometalates synthesized, are given in Table 1 and Table S1 in ESI†. For the V_x-BM_{50}-1_{BM}-1.5_{HT} materials, the x values obtained are very close to the theoretical values (less than 10% difference which can be related to the experimental error). In contrast, for the conventionally synthesized V_3-HT material, the difference between x_{exp} and x_{th} is more pronounced (>10%). Indeed, during the conventional hydrothermal synthesis of V_3-HT, a solid residue enriched in V_2O_5 had to be filtered before water evaporation, resulting unavoidably in a lower value of x_{exp}. These observations point to an improvement of the hydrothermal attack of the oxides favored by the ball-milling step.

Whatever the synthesis route, the TGA weight-losses for hydration (T_1 = 215–222 °C) and constitutive water (T_2 = 416–421 °C) took place at relatively similar temperatures for V_3-BM_{50}-1_{BM}-1.5_{HT} and V_3-HT (Fig. S2 and Table S3 in ESI†), showing that their vanadium contents are quite comparable. The hydration indexes (n) calculated from the TGA plots range between 12 and 15, and are in agreement with the results derived from the XRD analysis (Fig. 2a). Further insights into the purity and composition of the synthesized V_x were gained through liquid analyses. The ^{31}P NMR spectra acquired for V_2-BM_{50}-1_{BM}-1.5_{HT}, V_3-BM_{50}-1_{BM}-1.5_{HT} and V_3-HT are presented in Fig. 2b. These spectra are rather complex due to the presence of various isomers of V_3 in solution, the partial protonation of V_3 at pH ∼ 1 and the co-existence in solution of different V_x compounds (such as V_2) as previously shown in the literature by ^{31}P NMR.[34,35] First, based on the very similar values of x_{exp} and x_{th} obtained for V_2-BM_{50}-1_{BM}-1.5_{HT} and V_3-BM_{50}-1_{BM}-1.5_{HT}, respectively, and considering that H_3PO_4 is the only possible impurity, a synthesis yield was calculated, *i.e.* defined as the extent of H_3PO_4 incorporation into the V_x structures (calculated from the areas of the H_3PO_4 peaks in the ^{31}P NMR spectra, see details in the ESI†). The values of this synthesis yield were much higher for V_3-BM_{50}-1_{BM}-1.5_{HT} (97%) than those for V_3-HT (79%), pointing to a more effective incorporation of vanadium into $H_{3+x}[PMo_{12-x}V_xO_{40}]$ for the hybrid ball-milled/hydrothermal material in comparison with the conventionally synthesized one (Table 1).

For the lowest V-content (x_{th} = 2), the ^{31}P NMR spectrum obtained was relatively more simple, allowing us to get valuable information about the different isomers and V_x species present in V_2-BM_{50} (Table S4, see the ESI† for further details about these calculations). According to Pettersson,[34] six types of isomers could be identified in the ^{31}P NMR spectrum of V_2 polyoxometalates. The individual contributions of α-1,4 (−4.21 ppm, V atoms on the same triad), α-1,2 and α-1,5 (−4.03 ppm, vicinal V atoms on different triads), α-1,6 and α-1,11 (−3.94 ppm, no vicinity of V atoms) as well as β isomers (−3.77 ppm, most probably not vicinal β-4,10 and β-4,11 isomers,[34] Fig. S3 in the ESI†) with respect to the total amount of V_2 obtained are presented in Table S4.† In V_2-BM_{50}-1_{BM}-1.5_{HT}, the α-1,4 isomer was found to be present to a much greater extent than the other five possible isomers, *i.e.* α-1,4 amounts to 58.5% *vs.* 12.6% for α-1,2 and α-1,5, 16.3% for α-1,6 and α-1,11, and 12.7% for the β isomers. In fact, 71% of all the V_2 isomers in V_2-BM_{50}-1_{BM}-1.5_{HT} were shown to bear vicinal V atoms (α-1,4, α-1,2 and α-1,5, Table S4†). This information can be highly relevant for the application of these materials in catalysis, since previous studies evidenced that their activity in oxidation reactions can be directly linked to the presence of isomers bearing vicinal V atoms.[36]

The results presented so far prove that V_3 can be successfully obtained a with higher yield and with a much shorter synthesis time than conventionally prepared V_3-HT, when using r = 50 during the ball-milling step. Lowering the ball to oxide weight ratio will produce higher amounts of materials per synthesis batch. Therefore, we further considered the synthesis of V_x using r = 20 instead of 50, for x_{th} = 2, keeping the ball-milling and the hydrothermal attack (80 °C) duration constant. The x_{th} value of 2 was chosen due to the superior stability of V_2 in solution, *vis-à-vis* V_3, and for their easier characterization, especially by ^{31}P NMR. However, the resulting material, denoted as V_2-BM_{20}-1_{BM}-1.5_{HT}, did not exhibit the desired Keggin structure and an important H_3PO_4 signal was observed in its ^{31}P NMR spectrum (see Fig. S4 in the ESI†). Evidently, the 1 h milling time (t_{BM}) and the subsequent 1.5 h acid attack at 80 °C did not lead to a successful synthesis of V_2. Previous studies showed that an increased amount of powder in the ball-milling jar resulted in a thicker powder layer between the colliding entities,[37,38] thereby leading to a dramatic decrease of the local temperature during milling,[39,40] as a consequence of hindered heat transfer and more elastic shocks.[39–44] These experimental observations were even predicted mathematically, using the energy equation defined by Magini *et al.*[42] The duration of the ball-milling step (t_{BM}) was therefore increased

and the influence of both the duration (t_{HT}) and the temperature (T_{HT}) of the H_3PO_4 hydrothermal attack was further investigated. These experiments led to the formation of the second series of materials denoted as V_2-BM_{20}-t_{BM}-t_{HT}. First, the temperature of the acid attack was set to 100 °C (V_2-BM_{20}′-1_{BM}-1.5_{HT}), keeping the milling and attack durations unchanged. Then, while performing the H_3PO_4 attack at 80 °C, its duration was extended up to 3 h without modifying the duration of the milling step (1 h), affording the V_2-BM_{20}-1_{BM}-3_{HT} compound. In both cases, the recovered V_x materials showed the desired Keggin structure, as evidenced by their corresponding XRD profiles (Fig. S5 in the ESI†). Moreover, the absence of the signal of H_3PO_4 in the ^{31}P NMR spectra of V_2-BM_{20}′-1_{BM}-1.5_{HT} and V_2-BM_{20}-1_{BM}-3_{HT} proved that both syntheses were quantitative (Fig. S6 in the ESI†). Longer milling steps (t_{BM} = 2 or 4 h) were also assessed, affording the V_2-BM_{20}-2_{BM}-1.5_{HT}, V_2-BM_{20}-2_{BM}-3_{HT}, V_2-BM_{20}-4_{BM}-1.5_{HT} and V_2-BM_{20}-4_{BM}-3_{HT} materials. Very similar results in terms of structure and V_2 yields were obtained. For this V_2-BM_{20} series, the x_{exp} values determined from the ICP analyses and x_{th} values were at the best different from 1% (V_2-BM_{20}-2_{BM}-1.5_{HT}) and at worst 13% (V_2-BM_{20}-2_{BM}-3_{HT}, V_2-BM_{20}-4_{BM}-1.5_{HT}, and V_2-BM_{20}-1_{BM}-3_{HT}, see Table 1). TGA-DSC analyses of the V_2-BM_{20} materials (Fig. S7 in the ESI†) evidenced that the loss of constitutive water occurred almost at the same temperature (*ca.* T_2 = 428 °C, see Table S3†), corresponding to the hydration indexes, *n*, between 12 and 15. For the V_2-BM_{20} series, the yields ranged from 92 to 97% with the predominance of the α-1,4 isomer (37–48%), while the contribution of the isomers containing vicinal vanadium atoms remained quite high, between 61 and 65% (see Table S4†).

Energy consumption was further determined for both the hybrid synthesis route (BM–HT) and the 100% hydrothermal procedure (HT), using the methodology proposed by Hao and co-workers.[45] Briefly, considering that the main energy inputs are the ball-milling step itself and the heating process during the acid attack, the global energy consumption E_t (in kW h) can be calculated through the simple relation $E_t = P_{BM}t_{BM} + P_{HT}t_{HT}$, where P_{BM} and P_{HT} stand, respectively, for the power consumed during the milling step and during the acid attack (see Tables S5, 6 and the ESI† for further details). Based on the results obtained, the energy saving (in %) was calculated for each material, in comparison with the conventional hydrothermal route, *i.e.* V_3-HT (Table 2).

These values prove that the energy consumption during the hybrid synthesis is substantially reduced when compared to that involved in the conventional hydrothermal pathway for V_3-HT (see Table S5 in the ESI†). Energy savings up to almost 70% can be reached with the hybrid pathway (*i.e.* for V_2-BM_{20}′-1_{BM}-1.5_{HT} synthesis). This fact and the overall short synthesis time indicate that the hybrid milling-hydrothermal route can be a very prospective pathway for the preparation of V_x, with a high yield and purity.

Importance of the mechanochemical step: characterization of the ball-milled oxides

In order to gain deeper insight into the positive influence of the mechanochemical step in the overall procedure, the ball-milled mixtures, V_2-BM_{50}-1_{mix} (t_{BM} = 1 h, first series) and V_2-BM_{20}-t_{BMmix} (t_{BM} = 1, 2 or 4 h, second series) were recovered after the milling step (prior to the hydrothermal acid attack). They were subsequently characterized by XRD (Fig. 3a and Fig. S8, ESI†), Raman spectroscopy (Fig. 3b), SEM (Fig. 4a and b) and laser granulometry (Fig. 5).

The XRD patterns acquired for the ball-milled mixtures V_2-BM_{50}-1_{mix} and V_2-BM_{20}-t_{BMmix} are shown in Fig. 3a and

Table 2 Energy saving (in %) for different V_x synthesized including the ball-milling step *vs.* the one prepared through conventional hydrothermal synthesis

V_x	Energy saving (%)
V_3-HT	—[a]
V_3-BM_{50}-1_{BM}-1.5_{HT}	30
V_2-BM_{50}-1_{BM}-1.5_{HT}	31
V_2-BM_{20}′-1_{BM}-1.5_{HT}	68
V_2-BM_{20}-1_{BM}-3_{HT}	62
V_2-BM_{20}-2_{BM}-1.5_{HT}	54
V_2-BM_{20}-2_{BM}-3_{HT}	43
V_2-BM_{20}-4_{BM}-1.5_{HT}	19
V_2-BM_{20}-4_{BM}-3_{HT}	10

[a] Energy consumption: 627 kW h mol^{-1}. Details in Tables S5 and S6 (ESI†).

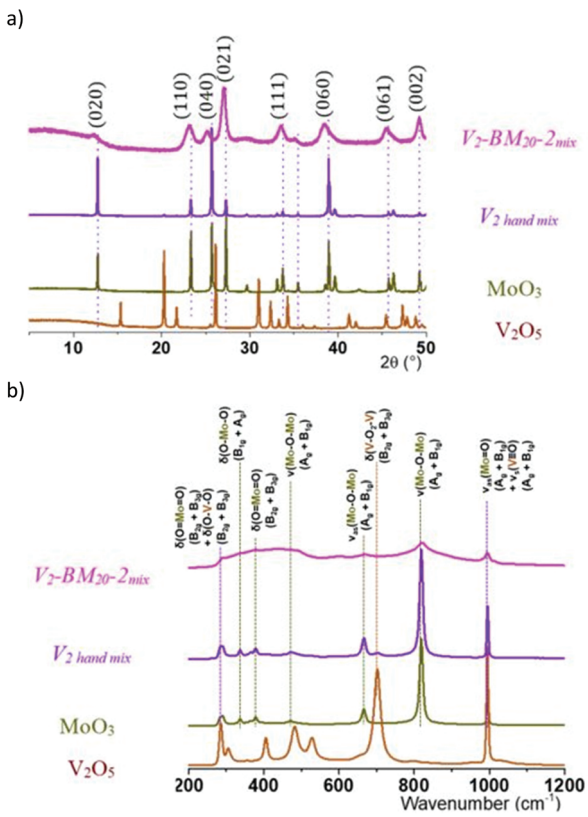

Fig. 3 (a) Powder-XRD patterns and (b) Raman spectra of the starting oxides (V_2O_5 and MoO_3), the hand-milled mixture $V_{2\ hand\ mix}$ and the ball-milled material V_2-BM_{20}-2_{mix}.

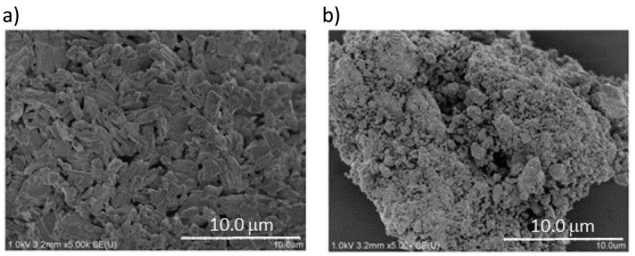

Fig. 4 SEM images (magnification ×5k) for (a) the hand-milled mixture, V_2 hand mix; (b) the ball-milled mixture, V_2-BM_{20}-2_{mix}.

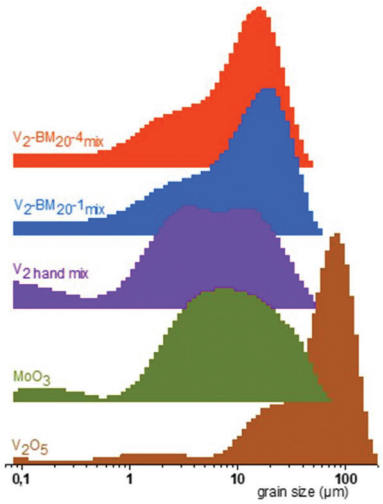

Fig. 5 Laser granulometry histograms for the starting oxides (V_2O_5 and MoO_3), the hand-milled mixture V_2 hand mix, and the ball-milled mixtures V_2-BM_{20}-1_{mix} and V_2-BM_{20}-4_{mix}.

Fig. S8.† These diffractogramms are presented together with the patterns of the starting V_2O_5 and MoO_3 oxides, as well as for a hand-milled mixture prepared with the same Mo/V ratio (V_2 hand mix). Both V_2O_5 (JCPDS 9-387, space group *Pmmn*) and MoO_3 (JCPDS 05-0508, space group *Pnma*) show an orthorhombic crystalline structure. Well-defined diffraction lines are observed for the hand-milled mixture V_2 hand mix. As expected, its XRD pattern is the result of the combination of the diffractograms of the parent MoO_3 and V_2O_5 oxides at a 1/8 V_2O_5/MoO_3 weight ratio (the reflections corresponding to V_2O_5 are scarcely perceptible). In contrast, the patterns acquired for the ball-milled oxides are characterized by the presence of wide diffraction signals and a less-well defined baseline. Crystallite sizes of 2.8 Å for V_2-BM_{50}-1_{mix} and around 1.4–1.7 Å for V_2-BM_{20}-t_{BMmix} were calculated from the widths at half peak height of the (110) diffraction (the Scherrer equation, shape factor $K = 0.888$, see details in the ESI†). These crystallite sizes are considerably smaller than those calculated for the hand-milled mixture of MoO_3 and V_2O_5 (Table S7, ESI†). This decrease in the crystallite size becomes more pronounced for the solids ball-milled at $r = 20$, whereas the duration of the milling step did not seem to affect the crystalline structure of the resulting mixtures. Moreover, the XRD reflections observed for the V_2-BM_{50}-1_{mix} and V_2-BM_{20}-t_{BMmix} ball-milled materials appear to be shifted to lower 2θ values, in comparison with those of pure MoO_3, pointing to the formation of a mixed-oxide phase. Molchanov *et al.*[28] suggested the formation of a mixed oxide upon ball-milling of the single starting V_2O_5 and MoO_3 oxides, although any experimental evidence supported their hypothesis.

Fig. 3b displays the Raman spectrum acquired for V_2-BM_{20}-2_{mix}, in comparison with the spectra registered for the starting oxides and for their hand-milled mixture. The Raman bands for pure MoO_3 [46,47] and pure V_2O_5 [48,49] can be seen in the spectrum of V_2-BM_{20}-2_{mix}. However, these bands appear broader, probably as a consequence of some structural disorder caused upon ball-milling.[50] In addition, the Raman spectrum of V_2-BM_{20}-2_{mix} shows several bands appearing between 200 and 600 cm^{-1}, which cannot be observed either for the hand-milled mixture or in the spectra of MoO_3 and V_2O_5. The presence of these bands further suggests the formation of a mixed oxide phase.[27] However, no significant shift in the position of the Raman bands corresponding to MoO_3 was observed, meaning that, in spite of the partial substitution of Mo by V within the crystalline network, the original structure of this oxide is well preserved upon ball-milling.

The representative SEM micrographs acquired for the hand-milled mixture V_2 hand mix and for the ball-milled mixture V_2-BM_{20}-2_{mix} are respectively presented in Fig. 4. The SEM image for the hand-mixed solid, Fig. 4a, evidences the presence of smooth particles having sizes *ca.* 2 × 0.6 µm, with quite regular elongated shapes that stuck together forming a relatively compact surface morphology.

Granular but more irregular structures are present in the SEM micrograph acquired for the ball-milled mixture V_2-BM_{20}-2_{mix}, Fig. 4b, pointing to some sintering occurring during the ball-milling step. The particles appear to be more agglomerated than those in the hand-milled mixture, and bigger particles (sizes up to 5 µm) can be easily observed. Sintering seemed to take place to a higher extent upon ball-milling at $r = 50$ (not shown). As previously commented, lower r ratios may result in lower local temperatures attained during milling,[42,43] disfavoring sintering and particle agglomeration.

In a further step, the grain size distribution in the different materials was assessed by laser granulometry (histograms shown in Fig. 5). The grain size distribution observed for the hand-milled material looks very similar to that of MoO_3, pointing to very similar grain sizes. In the case of the ball-milled oxides, V_2-BM_{20}-1_{mix} and V_2-BM_{20}-4_{mix}, the grain size distribution considerably changes with respect to the starting oxides. A bimodal grain size distribution is observed, composed of a main peak centered around 20 µm and a second population of smaller particle sizes around 2–5 µm. The grain distribution does not seem to change for longer ball-milling times, *i.e.* similar curves were obtained for V_2-BM_{20}-1_{mix} and for V_2-BM_{20}-4_{mix}. The ball-milling step alters not only the crystallinity of the solid but also its grain size, in complete agreement with the SEM observation of these materials. Sintering

occurs as a consequence of an increase of temperature in the ball-mill jar, yielding a solid consisting of particle aggregates with bigger sizes than those of the starting materials (mainly MoO_3).

Therefore, the XRD and Raman spectra are consistent with the formation of a Mo–V mixed oxide phase, probably due to the insertion of V cations into the original MoO_3 lattice. This does not lead to any dramatic change in the crystalline structure. However, higher crystallinity and smaller crystallite sizes were observed in the ball-milled solids, which may be a consequence of some sintering occurring during the ball-milling step. In spite of that, the surface of the ball-milled materials is rougher than that of MoO_3 or the hand-milled oxides (SEM analyses), which looks to be highly beneficial for the further acid attack with H_3PO_4, affording an easier synthesis of the V-substituted phosphomolybdic acids.

Activity and selectivity towards the C–C and C–O cleavage of the synthesized V_x materials

Simple lignin models have been often used in the screening of the catalysts and reaction conditions for lignin oxidative depolymerisation.[51] Among the very few reported contributions involving V_x, Evtuguin *et al.* studied the activity of V_5 as the catalyst for the aerobic cleavage of 1-(3-methoxy-4-hydroxyphenyl)-2-(2-methoxyphenoxy)ethanol (**1**) and 1-(3,4-dimethoxyphenyl)-2-(2-methoxyphenoxy)ethanol (**2**),[52,53] see Fig. 6. Ketone-type substrates such as benzoin (**3**), and, more interestingly, dimeric compounds such as 2-phenoxyacetophenone (**K**), have been considered as well,[4] since benzylic hydroxyl oxidation may occur *in situ* under aerobic oxidative conditions.[54]

We have recently proved that V_3-HT can be a very efficient catalyst for the aerobic cleavage of 2-phenoxyacetophenone **K**[4]. Here, we have evaluated the ability of the whole V_x series ($1.9 < x_{exp} < 2.8$) prepared through the hybrid ball-milling/hydrothermal route to catalyze the aerobic cleavage of C–C and C–O bonds in **K**. The activity and selectivity of the $PMoV_x$-BM–HT materials were compared to those of conventionally synthesized V_3-HT, with emphasis on possible correlations with their respective physicochemical properties.

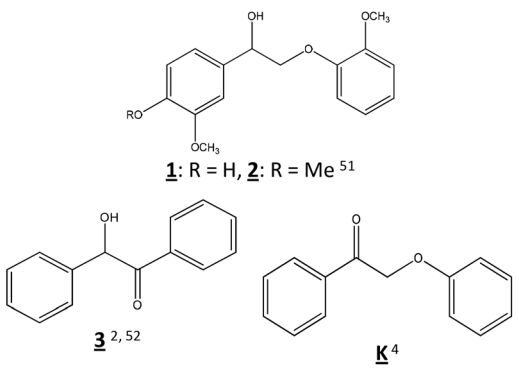

Fig. 6 Dimeric aromatic molecules studied as substrates in the phosphomolybdic acid catalyzed aerobic cleavage reaction.

The cleavage experiments were carried out in MeCN/AcOH, at 82 °C under an atmospheric pressure of O_2 during 24 h (optimal reaction conditions, identified in our previous work[4]). The catalyst loading was fixed at 18 mol% with respect to Mo and V, according to the available literature on aerobic delignification involving $H_3PMo_{12}O_{40}$ as a catalyst.[55] Under such reaction conditions the oxidation of **K** affords mainly phenol (PhOH) from C–O cleavage, benzaldehyde (PhCHO) and benzoic acid (PhCOOH) from the C–C cleavage (see Fig. 7, as well as the HPLC analyses presented in Fig. S9, ESI†).

Table 3 shows the conversion, product yield and carbon balance (CB) values determined during the aerobic cleavage of **K** in the presence of the different synthesized V_x materials.

For V contents corresponding to $x = 3$, the material V_3-BM_{50}-1_{BM}-1.5_{HT} (entry 2) evidenced catalytic performance similar to that of conventionally synthesized V_3-HT (entry 1). However, a slightly higher **K** conversion was observed in the presence of the catalyst obtained through the hybrid ball-milling/hydrothermal procedure (78% *vs.* 72% for V_3-HT), together with lower carbon balance values, probably due to phenol degradation.

Within the first series of hybrid BM–HT materials, V_2-BM_{50}-1_{BM}-1.5_{HT} (entry 3) led to the highest **K** conversion (84% *vs.* 78% for V_3-BM_{50}-1_{BM}-1.5_{HT}), along with high yields of phenol (54%), benzaldehyde (19%) and benzoic acid (49%), while maintaining a correct carbon balance. Even with a lower V content ($x = 2$ instead of 3), V_2-BM_{50}-1_{BM}-1.5_{HT} evidenced improved catalytic performance compared to its counterpart and V_3-HT, the conventionally synthesized material which is rather unusual, since the oxidation potential is expected to increase with x but it is also known that V_3 materials are less stable in solution than their V_2 analogs and are found to be deactivated earlier.[56]

For the series of V_2-BM_{20}-t_{BM}-t_{HT} materials (entries 4–9), conversions between 70 and 81% were obtained. As previously reported,[4] the carbon balance values decrease with increasing conversion, due to a higher extent of oxidation that may sometimes be not very selective. At $x = 2$, this lack of selectivity seems to affect mostly the yield of benzaldehyde, as observed for V_2-BM_{20}-4_{BM}-3_{HT}, entry 9 (7% PhCHO yield and a carbon balance of 67% which is the lowest CB value of this series). However, no direct relationship can be established between the synthesis parameters (duration of the milling step and hydrothermal attack) and the catalytic performance of these materials. The average values were calculated, indicating that the six samples of the V_2-BM_{20}-t_{BM}-t_{HT} series afforded similar conversions and yields. For these V_2-BM_{20}-t_{BM}-t_{HT}, no evident correlation can be drawn between the relative presence of the α-1,4 isomer and their catalytic activity and selectivity.

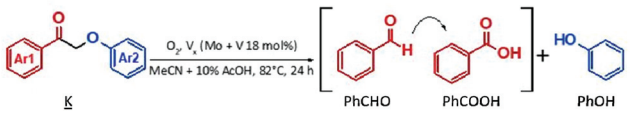

Fig. 7 Aerobic cleavage of **K**.

Table 3 Aerobic cleavage of **K** in the presence of different synthesized V_x: conversion, product yield and carbon balance. The amounts (in percentage) of the α-1,4 isomer, calculated from the liquid ^{31}P NMR spectra, are also shown for each catalyst

				HPLC yield, η (%)			
					C–C cleavage		
Entry	Catalyst	α-1,4 Isomer (%)	Conversion (%)	PhOH	PhCHO	PhCOOH[a] (Σ)	CB[b] (%)
1	V_3-HT	n.d.	72	52	12	42 (54)	77
2	V_3-BM_{50}-1_{BM}-1.5_{HT}	n.d.	78	38	16	32 (48)	62
3	V_2-BM_{50}-1_{BM}-1.5_{HT}	58.5	84	54	19	49 (68)	78
4	V_2-BM_{20}'-1_{BM}-1.5_{HT}	47.9	77	48	14	38 (52)	70
5	V_2-BM_{20}-1_{BM}-3_{HT}	42.2	81	42	17	47 (64)	69
6	V_2-BM_{20}-2_{BM}-1.5_{HT}	49.1	70	57	23	31 (54)	81
7	V_2-BM_{20}-2_{BM}-3_{HT}	46.0	75	37	15	38 (53)	67
8	V_2-BM_{20}-4_{BM}-1.5_{HT}	45.2	79	52	12	41 (53)	70
9	V_2-BM_{20}-4_{BM}-3_{HT}	37.4	81	59	7	39 (46)	67
	Average V_2-BM_{20}[c]	*45 ± 3*	*77 ± 3*	*49 ± 5*	*15 ± 3*	*39 ± 3*	*71 ± 3*

K 100 mM, atm. O_2, Mo + V 18 mol%, MeCN + 10 vol% AcOH, 82 °C, 24 h. [a] $\Sigma = \eta_{PhCHO} + \eta_{PhCOOH}$. [b] Calculated as CB = $(6\eta_{PhOH} + 7(\eta_{PhCHO} + \eta_{PhCOOH}) + 14(100 - conv.))/14 < 100\%$, since C_1 products from the oxidation of the CH_2 group in **K** were not quantified. [c] Average values for the six V_2-BM_{20} materials. Confidence limit = 80%; n.d.: not determined.

However, V_2-BM_{50}-1_{BM}-1.5_{HT} for which the highest conversion was observed among all the materials, shows the highest relative amount of the α-1,4 isomer (58.5%), which seems to lead to a somehow enhanced selectivity towards C–C cleavage ($\Sigma = \eta_{PhCHO} + \eta_{PhCOOH}$ amounts to 68%, whereas the C–C global yield determined for V_2-BM_{20}-4_{BM}-3_{HT} was only 46% for a α-1,4 isomer content of 37.4%). In this sense, a shorter ball-milling step at $r = 50$ seems to be more beneficial in terms of catalytic activity and C–C– cleavage selectivity than that at $r = 20$ at longer milling and attack durations, since the presence of the α-1,4 isomer seems to be moreover favoured.

Let us note here that the spent V_3-HT catalyst was previously characterized by ^{31}P NMR.[4] In brief, the Keggin structure was shown to be unstable upon reduction by the substrate. As a consequence, the V_x compound dissociates into pervanadyl cations VO_2^+ and into other unstable lacunary species, which are most probably the catalytically active species in oxidative cleavage reactions. In the case of V_2, the release of pervanadyl cations is favored by the presence of vicinal vanadium atoms as in the α-1,4 isomer,[57] which may therefore explain their improved catalytic activity, particularly towards C–C cleavage.

Conclusions

A series of vanadium-substituted phosphomolybdic acids, V_x, were successfully synthesized through a hybrid mechanochemical/hydrothermal route, involving a ball-milling step, followed by subsequent H_3PO_4 attack. The resulting solids showed the typical Keggin structure of V_x materials. Their hydration indexes were very similar to those observed in the reference material prepared through a conventional hydrothermal route. High V_x yields were obtained, as a consequence of the formation of a highly crystalline Mo–V mixed-oxide in the milling step, exhibiting surface rugosity that facilitated the acid attack.

The different V_x materials synthesized were used as catalysts for the aerobic cleavage of C–O and C–C bonds in a dimeric lignin model (**K**). Generally, the materials prepared through the hybrid mechanochemical/hydrothermal route, with $2 < x_{exp} < 3$, exhibited slightly improved catalytic performance compared to the conventionally synthesized V_3-HT. Among them, V_2-BM_{50}-1_{BM}-1.5_{HT}, obtained through the hybrid route comprising a ball-milling step performed with a ball/oxide weight ratio $r = 50$ for 1 h and a 1.5 h-acid attack of the ball-milled mixture, afforded higher **K** conversion than V_3-HT, *i.e.* 84% *vs.* 72%. Moreover, this material showed improved selectivity towards C–C cleavage, which was related to an increased amount of the α-1,4 isomer, as determined from the analysis of the liquid ^{31}P NMR spectra.

Therefore, the hybrid mechanochemical/hydrothermal route explored in the present work allowed us to obtain V_x with high yields and a short synthesis time, with respect to a conventional hydrothermal procedure. This route can provide up to 68% energy saving, yielding materials with very promising applications in lignin oxidative depolymerization reactions.

Author contributions

LAH, MEG and FL have equally contributed to the research presented herein. All the authors have equally contributed to the writing of the manuscript. All the authors have agreed to its submission for publication and accepted the responsibility for having properly included all (and only) co-authors.

Conflicts of interest

There are no conflicts to declare.

Acknowledgements

We gratefully acknowledge the Program "Génie des Procédés" at Sorbonne Université for the Ph.D fellowship (2016-2019) of L. Al-Hussaini, as well as Sorbonne Université, the European Union (ERDF) and the CNRS for their financial support. We would like to thank Mohamed Selmane, Claire Troufflard, and Aurélie Bernard, Jean-Marc Krafft and Sandra Casale for XRD, NMR, Raman and SEM characterization.

Notes and references

1 I. A. Weinstock, R. E. Schreiber and R. Neumann, *Chem. Rev.*, 2018, **118**, 2680–2717.
2 L. El Aakel, F. Launay, J.-M. Brégeault and A. Atlamsani, *Chem. Commun.*, 2001, 2218–2219.
3 A. R. Gaspar, J. A. F. Gamelas, D. V. Evtuguin and C. P. Neto, *Green Chem.*, 2007, **9**, 717–730.
4 L. Al-Hussaini, F. Launay and E. Gálvez, *Materials*, 2020, **13**, 812–833.
5 C. Liu, S. Wu, H. Zhang and R. Xiao, *Fuel Process. Technol.*, 2019, **191**, 181–201.
6 G. A. Tsigdinos and J. Hallada, *Inorg. Chem.*, 1968, **7**, 437–441.
7 F. Kern, S. Ruf and G. Emig, *Appl. Catal., A*, 1997, **150**, 143–151.
8 T. Onoda and T. Otake, Pat. US4146574, 1979.
9 V. F. Odyakov and E. G. Zhizhina, *Russ. J. Inorg. Chem.*, 2009, **54**, 361–367.
10 J. Qu, L. Sha, C. Wu and Q. Zhang, *Nanomaterials*, 2019, **9**, 80–94.
11 J. G. Hernández and T. Frišić, *Tetrahedron Lett.*, 2015, **56**, 4253–4265.
12 Z. Wang, Z. Li, M. Ng and P. J. Milner, *Dalton Trans.*, 2020, **49**, 16238–16244.
13 F. Preishuber-Pflügl and M. Wilkening, *Dalton Trans.*, 2016, **45**, 8675–8687.
14 N. Pétry, H. Benakki, E. Clot, P. Retailleau, F. Guenoun, F. Asserar, C. Sekkat, T.-X. Métro, J. Martinez and F. Lamaty, *Beilstein J. Org. Chem.*, 2017, **13**, 2169–2178.
15 A. Beillard, X. Bantreil, T.-X. Métro, J. Martinez and F. Lamaty, *Chem. Rev.*, 2019, **119**, 7529–7609.
16 V. Šepelák, S. Bégin-Colin and G. Le Caër, *Dalton Trans.*, 2012, **41**, 11927–11948.
17 E. Gil-González, A. Perejón, P. E. Sánchez-Jiménez, M. A. Hayward and L. A. Pérez-Maqueda, *J. Eur. Ceram. Soc.*, 2017, **37**, 945–954.
18 P. Opitz, M. P. Asta, A. Fernandez-Martinez, M. Panthöfer, A. Kabelitz, F. Emmerling, M. Mondeshki and W. Tremel, *Cryst. Growth Des.*, 2020, **20**, 6831–6846.
19 M. Liu, L. Wang, K. Zhao, S. Shi, Q. Shao, L. Zhang, X. Sun, Y. Zhao and J. Zhang, *Energy Environ. Sci.*, 2019, **12**, 2890–2923.
20 J. Li, C. Lai, X. Jia, L. Wang, X. Xiang, C.-L. Ho, H. Li and W.-Y. Wong, *Composites, Part B*, 2015, **77**, 248–256.
21 N. R. Rightmire and T. P. Hanusa, *Dalton Trans.*, 2016, **45**, 2352–2362.
22 S. Leukel, M. Panthöfer, M. Mondeshki, G. Kieslich, Y. Wu, N. Krautwurst and W. Tremel, *Chem. Mater.*, 2018, **30**(17), 6040–6052.
23 L. Takacs, *Prog. Mater. Sci.*, 2002, **47**, 355–414.
24 C. Xu, S. De, A. M. Balu, M. Ojeda and R. Luque, *Chem. Commun.*, 2015, **51**, 6698–6713.
25 H. Lyu, B. Gao, F. He, C. Ding, J. Tang and J. C. Crittenden, *ACS Sustainable Chem. Eng.*, 2017, **5**, 9568–9585.
26 M. J. Muñoz-Batista, D. Rodriguez-Padron, A. R. Puente-Santiago and R. Luque, *ACS Sustainable Chem. Eng.*, 2018, **6**, 9530–9544.
27 V. A. Zazhigalov, S. V. Khalameida, N. S. Litvin, I. V. Bacherikova, J. Stoch and L. Depero, *Kinet. Catal.*, 2008, **49**, 692–701.
28 V. V. Molchanov, G. M. Maksimov, R. I. Maksimovskaya, V. V. Goidin and R. A. Buyanov, *Inorg. Mater.*, 2003, **39**, 687–693.
29 L. Xu, Y. Wang, T. Xu, S. Liu, J. Tong, R. Chu, X. Hou and B. Liu, *ChemCatChem*, 2018, **10**, 5386–5390.
30 Y. Leng, Y. Jiang, H. Peng, Z. Zhang, M. Liu, K. Jie, P. Zhang and S. Dai, *Catal. Sci. Technol.*, 2019, **9**, 2173–2179.
31 J. She, Z. Fu, J. Li, B. Zeng, S. Tang, W. Wu, H. Zhao, D. Yin and S. R. Kirk, *Appl. Catal., B*, 2016, **182**, 392–404.
32 P. Mothé-Esteves, M. Maciel Pereira, J. Arichi and B. Louis, *Cryst. Growth Des.*, 2010, **10**, 371–378.
33 D. Barats-Damatov, L. J. W. Shimon, Y. Feldman, T. Bendikov and R. Neumann, *Inorg. Chem.*, 2015, **54**, 628–634.
34 L. Pettersson, *Mol. Eng.*, 1993, **3**, 29–42.
35 L. Pettersson, I. Andersson, A. Selling and J. H. Grate, *Inorg. Chem.*, 1994, **33**, 982–993.
36 R. Neumann and A. Khenkin, *Chem. Commun.*, 2006, 2529–2538.
37 D. R. Maurice and T. H. Courtney, *Metall. Mater. Trans. A*, 1990, **21**, 289–303.
38 S.-Y. Lu, M. Q.-J. Mao, Z. Peng, X.-D. Li and J.-H. Yan, *Chin. Phys. B*, 2012, **21**, 078201–078209.
39 Y.-S. Kwon, K. B. Gerasimov and S.-K. Yoon, *J. Alloys Compd.*, 2002, **346**, 276–281.
40 R. Schmidt, H. M. Scholze and A. Stolle, *Int. J. Ind. Chem.*, 2016, **7**, 181–186.
41 G. Mulas, L. Schiffini and G. Cocco, *Mater. Sci. Forum*, 1996, **225**, 237–242.
42 M. Magini, A. Iasonna and F. Padella, *Scr. Mater.*, 1996, **34**, 13–19.
43 L. Takacs and J. S. McHenry, *J. Mater. Sci.*, 2006, **41**, 5246–5249.
44 P. P. Chattopadhyay, I. Manna, S. Talapatra and S. K. Pabi, *Mater. Chem. Phys.*, 2001, **68**, 85–94.
45 L. Hao, Y. Lu, H. Sato, H. Asanuma and J. Luo, *Int. J. Miner. Process.*, 2013, **121**, 51–58.
46 G. Mestl, P. Ruiz, B. Delmon and H. Knozinger, *J. Phys. Chem.*, 1994, **98**, 11269–11275.

47 D. Liu, W. W. Lei, J. Hao, D. D. Liu, B. B. Liu, X. Wang, X. H. Chen, Q. L. Cui, G. T. Zou, J. Liu and S. Jiang, *J. Appl. Phys.*, 2009, **105**, 023513.
48 L. Abello, E. Husson, Y. Repelin and G. Lucazeau, *Spectrochim. Acta, Part A*, 1983, **39A**, 64l–651.
49 F. D. Hardcastle and I. E. Wachs, *J. Phys. Chem.*, 1991, **95**, 5031–5041.
50 E. Skwarek, S. Khalameida, W. Janusz, V. Sydorchuk, N. Konovalova, V. Zazhigalov, J. Skubiszewska-Zięba and R. Leboda, *J. Therm. Anal. Calorim.*, 2011, **106**, 881–894.
51 J. Zakzeski, P. C. A. Bruijnincx, A. L. Jongerius and B. M. Weckhuysen, *Chem. Rev.*, 2010, **110**, 3552–3599.
52 D. V. Evtuguin, A. I. D. Daniel, A. J. D. Silvestre, F. M. L. Amado and C. P. Neto, *J. Mol. Catal. A: Chem.*, 2000, **154**, 217–224.
53 M. Wang, J. Ma, H. Liu, N. Luo, Z. Zhao and F. Wang, *ACS Catal.*, 2018, **8**, 2129–2165.
54 Y. Ma, Z. Du, J. Liu, F. Xia and J. Xu, *Green Chem.*, 2015, **17**, 4968–4973.
55 T. Voitl and P. R. von Rohr, *Ind. Eng. Chem. Res.*, 2010, **64**, 520–525.
56 I. V. Kozhevnikov, *Chem. Rev.*, 1998, **98**, 171–198.
57 M. J. Janik, B. B. Bardin, R. J. Davis and M. Neurock, *J. Phys. Chem. B*, 2006, **110**, 4170–4178.